Chapter 25

Relaxation for cyclists

Cycles, that is, solutions of the periodic orbit condition (14.1)

$$f^{t+T}(x) = f^t(x)\,, \qquad T > 0 \tag{25.1}$$

are prerequisite to chapters 11 and 12 evaluation of spectra of classical evolution operators, and, as we shall see in chapter 27, the semiclassical approximations to quantum evolution operators. Chapter 14 offered an introductory, hands-on guide to extraction of periodic orbits by means of the Newton-Raphson method. Here we take a very different tack, drawing inspiration from variational principles of classical mechanics, and path integrals of quantum mechanics.

In sect. 14.2.1 we converted orbits unstable forward in time into orbits stable backwards in time. Indeed, all methods for finding unstable cycles are based on the idea of constructing a new dynamical system such that (i) the position of the cycle is the same for the original system and the transformed one, (ii) the unstable cycle in the original system is a stable cycle of the transformed system.

The Newton-Raphson method for determining a fixed point x_* for a map $x' = f(x)$ is an example. The method replaces iteration of $f(x)$ by iteration of the Newton-Raphson map (14.5)

$$x'_i = g_i(x) = x_i - \left(\frac{1}{\mathbf{J}(x) - \mathbf{1}}\right)_{ij} (f(x) - x)_j\,. \tag{25.2}$$

A fixed point x_* for a map $f(x)$ is also a fixed point of $g(x)$, indeed a super-stable fixed point since $\partial g_i(x_*)/\partial x_j = 0$. This makes the convergence to the fixed point super-exponential.

We also learned in chapter 14 that methods that start with initial guesses for a number of points along a cycle are considerably more robust and safer than searches based on direct solution of the fixed-point condition (25.1). The relaxation (or variational) methods that we shall now describe take this multipoint approach to its logical extreme, and start by a guess of not a few points along a periodic orbit, but a guess of the entire orbit.

The idea is to make an informed rough guess of what the desired periodic orbit looks like globally, and then use variational methods to drive the initial guess toward the exact solution. Sacrificing computer memory for robustness of the method, we replace a guess that a *point* is on the periodic orbit by a guess of the *entire orbit*. And, sacrificing speed for safety, in sect. 25.1 we replace the Newton-Raphson *iteration* by a fictitious time *flow* that minimizes a cost function computed as deviation of the approximate flow from the true flow along a loop approximation to a periodic orbit.

If you have some insight into the topology of the flow and its symbolic dynamics, or have already found a set of short cycles, you might be able to construct an initial approximation to a longer cycle p as a sequence of N points $(\tilde{x}_1^{(0)}, \tilde{x}_2^{(0)}, \cdots, \tilde{x}_N^{(0)})$ with the periodic boundary condition $\tilde{x}_{N+1} = \tilde{x}_1$. Suppose you have an iterative method for improving your guess; after k iterations the cost function

$$F^2(\tilde{x}^{(k)}) = \sum_i^N \left(\tilde{x}_{i+1}^{(k)} - f(\tilde{x}_i^{(k)})\right)^2 \tag{25.3}$$

or some other more cleverly constructed function (for classical mechanics - action) is a measure of the deviation of the kth approximate cycle from the true cycle. This observation motivates variational approaches to determining cycles.

We give here three examples of such methods, two for maps, and one for billiards. In sect. 25.1 we start out by converting a problem of finding an unstable fixed point of a map into a problem of constructing a differential flow for which the desired fixed point is an attracting equilibrium point. Solving differential equations can be time intensive, so in sect. 25.2 we replace such flows by discrete iterations. In sect. 25.3 we show that for $2D$-dimensional billiard flows variation of D coordinates (where D is the number of Hamiltonian degrees of freedom) suffices to determine cycles in the full $2D$-dimensional phase space.

25.1 Fictitious time relaxation

(O. Biham, C. Chandre and P. Cvitanović)

The relaxation (or gradient) algorithm for finding cycles is based on the observation that a trajectory of a map such as the Hénon map (3.10),

$$\begin{aligned} x_{i+1} &= 1 - ax_i^2 + by_i \\ y_{i+1} &= x_i \,, \end{aligned} \tag{25.4}$$

is a stationary solution of the relaxation dynamics defined by the flow

$$\frac{dx_i}{d\tau} = v_i, \quad i = 1, \ldots, n \tag{25.5}$$

for any vector field $v_i = v_i(x)$ which vanishes on the trajectory. Here τ is a "fictitious time" variable, unrelated to the dynamical time (in this example, the discrete time of map iteration). As the simplest example, take v_i to be the deviation of an approximate trajectory from the exact 2-step recurrence form of the Hénon map (3.11)

$$v_i = x_{i+1} - 1 + ax_i^2 - bx_{i-1}. \tag{25.6}$$

For fixed x_{i-1}, x_{i+1} there are two values of x_i satisfying $v_i = 0$. These solutions are the two extremal points of a local "potential" function (no sum on i)

$$v_i = \frac{\partial}{\partial x_i} V_i(x) \,, \qquad V_i(x) = x_i(x_{i+1} - bx_{i-1} - 1) + \frac{a}{3} x_i^3 \,. \tag{25.7}$$

Assuming that the two extremal points are real, one is a local minimum of $V_i(x)$ and the other is a local maximum. Now here is the idea; replace (25.5) by

$$\frac{dx_i}{d\tau} = \sigma_i v_i, \quad i = 1, \ldots, n, \tag{25.8}$$

where $\sigma_i = \pm 1$.

The modified flow will be in the direction of the extremal point given by the local maximum of $V_i(x)$ if $\sigma_i = +1$ is chosen, or in the direction of the one corresponding to the local minimum if we take $\sigma_i = -1$. This is not quite what happens in solving (25.8) - all x_i and $V_i(x)$ change at each integration step - but this is the observation that motivates the method. The differential equations (25.8) then drive an approximate initial guess toward the exact trajectory. A sketch of the landscape in which x_i converges

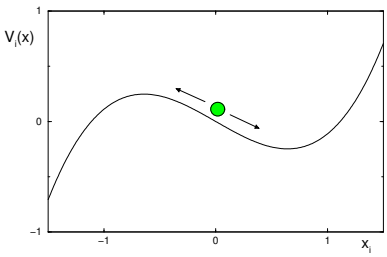

Figure 25.1: "Potential" $V_i(x)$ (25.7) for a typical point along an inital guess trajectory. For $\sigma_i = +1$ the flow is toward the local maximum of $V_i(x)$, and for $\sigma_i = -1$ toward the local minimum. A large deviation of x_i's is needed to destabilize a trajectory passing through such local extremum of $V_i(x)$, hence the basin of attraction is expected to be large.

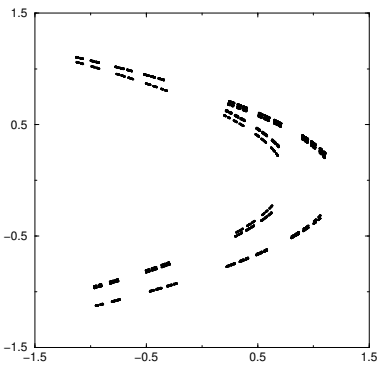

Figure 25.2: The repeller for the Hénon map at $a = 1.8$, $b = 0.3$.

towards the proper fixed point is given in fig. 25.1. As the "potential" function (25.7) is not bounded for a large $|x_i|$, the flow diverges for initial guesses which are too distant from the true trajectory. However, the basin of attraction of initial guesses that converge to a given cycle is nevertheless very large, with the spread in acceptable initial guesses for fig. 25.1 of order 1, in contrast to the exponential precision required of initial guesses by the Newton-Raphson method.

Example 25.1 Hénon map cycles. *Our aim in this calculation is to find all periodic orbits of period n for the Hénon map (25.4), in principle at most 2^n orbits. We start by choosing an initial guess trajectory $(x_1, x_2, \cdots, x_n)$ and impose the periodic boundary condition $x_{n+1} = x_1$. The simplest and a rather crude choice of the initial condition in the Hénon map example is $x_i = 0$ for all i. In order to find a given orbit one sets $\sigma_i = -1$ for all iterates i which are local minima of $V_i(x)$, and $\sigma_i = 1$ for iterates which are local maxima. In practice one runs through a complete list of prime cycles, such as the table 9.2. The real issue for all searches for periodic orbits, this one included, is how large is the basin of attraction of the desired periodic orbit? There is no easy answer to this question, but empirically it turns out that for the Hénon map such initial guess almost always converges to the desired trajectory as long as the initial $|x|$ is not too large compared to $1/\sqrt{a}$. Fig. 25.1 gives some indication of a typical basin of attraction of the method (see also fig. 25.3).*

The calculation is carried out by solving the set of n ordinary differential equations (25.8) using a simple Runge-Kutta method with a relatively large step size ($h = 0.1$) until $|v|$ becomes smaller than a given value ε (in a typical calculation $\varepsilon \sim 10^{-7}$). Empirically, in the case that an orbit corresponding to the desired itinerary does not exist, the initial guess escapes to infinity since the "potential" $V_i(x)$ grows without bound.

25.3
page 479

n	p	(y_p , x_p)	λ_p
1	0	(-1.13135447 , -1.13135447)	1.18167262
	1	(0.63135447 , 0.63135447)	0.65427061
2	01	(0.97580005 , -0.47580005)	0.55098676
4	0111	(-0.70676677 , 0.63819399)	0.53908457
6	010111	(-0.41515894 , 1.07011813)	0.55610982
	011111	(-0.80421990 , 0.44190995)	0.55245341
7	0011101	(-1.04667757 , -0.17877958)	0.40998559
	0011111	(-1.08728604 , -0.28539206)	0.46539757
	0101111	(-0.34267842 , 1.14123046)	0.41283650
	0111111	(-0.88050537 , 0.26827759)	0.51090634
8	00011101	(-1.25487963 , -0.82745422)	0.43876727
	00011111	(-1.25872451 , -0.83714168)	0.43942101
	00111101	(-1.14931330 , -0.48368863)	0.47834615
	00111111	(-1.14078564 , -0.44837319)	0.49353764
	01010111	(-0.52309999 , 0.93830866)	0.54805453
	01011111	(-0.38817041 , 1.09945313)	0.55972495
	01111111	(-0.83680827 , 0.36978609)	0.56236493
9	000111101	(-1.27793296 , -0.90626780)	0.38732115
	000111111	(-1.27771933 , -0.90378859)	0.39621864
	001111101	(-1.10392601 , -0.34524675)	0.51112950
	001111111	(-1.11352304 , -0.36427104)	0.51757012
	010111111	(-0.36894919 , 1.11803210)	0.54264571
	011111111	(-0.85789748 , 0.32147653)	0.56016658
10	0001111101	(-1.26640530 , -0.86684837)	0.47738235
	0001111111	(-1.26782752 , -0.86878943)	0.47745508
	0011111101	(-1.12796804 , -0.41787432)	0.52544529
	0011111111	(-1.12760083 , -0.40742737)	0.53063973
	0101010111	(-0.48815908 , 0.98458725)	0.54989554
	0101011111	(-0.53496022 , 0.92336925)	0.54960607
	0101110111	(-0.42726915 , 1.05695851)	0.54836764
	0101111111	(-0.37947780 , 1.10801373)	0.56915950
	0111011111	(-0.69555680 , 0.66088560)	0.54443884
	0111111111	(-0.84660200 , 0.34750875)	0.57591048
13	1110011101000	(-1.2085766485 , -0.6729999948)	0.19882434
	1110011101001	(-1.0598110494 , -0.2056310390)	0.21072511

Table 25.1: All prime cycles up to period 10 for the Hénon map, $a = 1.4$ and $b = 0.3$. The columns list the period n_p, the itinerary (defined in remark 25.4), a cycle point (y_p, x_p), and the cycle Lyapunov exponent $\lambda_p = \ln|\Lambda_p|/n_p$. While most of the cycles have $\lambda_p \approx 0.5$, several significantly do not. The $\overline{0}$ cycle point is very unstable, isolated and transient fixed point, with no other cycles returning close to it. At period 13 one finds a pair of cycles with exceptionally low Lyapunov exponents. The cycles are close for most of the trajectory, differing only in the one symbol corresponding to two cycle points straddle the (partition) fold of the attractor. As the system is not hyperbolic, there is no known lower bound on cycle Lyapunov exponents, and the Hénon's strange "attractor" might some day turn out to be nothing but a transient on the way to a periodic attractor of some long period.

n	M_n	N_n	n	M_n	N_n	n	M_n	N_n
11	14	156	17	166	2824	23	1930	44392
12	19	248	18	233	4264	24	2902	69952
13	32	418	19	364	6918	25	4498	112452
14	44	648	20	535	10808	26	6806	177376
15	72	1082	21	834	17544	27	10518	284042
16	102	1696	22	1225	27108	28	16031	449520

Table 25.2: The number of unstable periodic orbits of the Hénon map for $a = 1.4$, $b = 0.3$, of all periods $n \leq 28$. M_n is the number of prime cycles of length n, and N_n is the total number of periodic points of period n (including repeats of shorter prime cycles).

Applied to the Hénon map at the Hénon's parameters choice $a = 1.4$, $b = 0.3$, the method has yielded all periodic orbits to periods as long as $n = 28$, as well as selected orbits up to period $n = 1000$. All prime cycles up to period 10 for the Hénon map, $a = 1.4$ and $b = 0.3$, are listed in table 25.1. The number of unstable periodic orbits for periods $n \leq 28$ is given in table 25.2. Comparing this with the list of all possible 2-symbol alphabet prime cycles, table 9.2, we see that the pruning is quite extensive, with the number of cycle points of period n growing as $e^{0.4645 \cdot n} = (1.592)^n$ rather than as 2^n.

As another example we plot all unstable periodic points up to period $n = 14$ for $a = 1.8$, $b = 0.3$ in fig. 25.2. Comparing this repelling set with the strange attractor for the Hénon's parameters fig. 3.4, we note the existence of gaps in the set, cut out by the preimages of the escaping regions.

☞ remark 25.2

In practice, the relaxation flow (25.8) finds (almost) all periodic orbits which exist and indicates which ones do not. For the Hénon map the method enables us to calculate almost all unstable cycles of essentially any desired length and accuracy.

The idea of the relaxation algorithm illustrated by the above Hénon map example is that instead of searching for an unstable periodic orbit of a map, one searches for a stable attractor of a vector field. More generally, consider a d-dimensional map $x' = f(x)$ with a hyperbolic fixed point x_*. Any fixed point x_* is by construction an equilibrium point of the fictitious time flow

$$\frac{dx}{d\tau} = f(x) - x. \tag{25.9}$$

If all eigenvalues of the Jacobian matrix $J(x_*) = Df(x_*)$ have real parts smaller than unity, then x_* is a stable equilibrium point of the flow.

If some of the eigenvalues have real parts larger than unity, then one needs to modify the vector field so that the corresponding directions of the flow are turned into stable directions in a neighborhood of the fixed point. In the spirit of (25.8), modify the flow by

$$\frac{dx}{d\tau} = \mathbf{C}\left(f(x) - x\right), \tag{25.10}$$

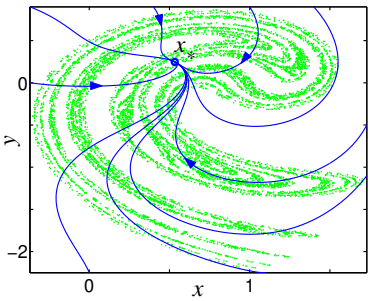

Figure 25.3: Typical trajectories of the vector field (25.9) for the stabilization of a hyperbolic fixed point of the Ikeda map (25.11) located at $(x, y) \approx (0.53275, 0.24689)$. The circle indicates the position of the fixed point. Note that the basin of attraction of this fixed point is large, larger than the entire Ikeda attractor.

where $\mathbf{C}$ is a $[d \times d]$ invertible matrix. The aim is to turn x_* into a stable equilibrium point of the flow by an appropriate choice of $\mathbf{C}$. It can be shown that a set of permutation / reflection matrices with one and only one non-vanishing entry ± 1 per row or column (for d-dimensional systems, there are $d!2^d$ such matrices) suffices to stabilize any fixed point. In practice, one chooses a particular matrix $\mathbf{C}$, and the flow is integrated. For each choice of $\mathbf{C}$, one or more hyperbolic fixed points of the map may turn into stable equilibria of the flow.

appendix G.2

Example 25.2 Ikeda map. *We illustrate the method with the determination of the periodic orbits of the Ikeda map:*

$$\begin{aligned} x' &= 1 + a(x\cos w - y\sin w) \\ y' &= a(x\sin w + y\cos w) \\ \text{where}\quad w &= b - \frac{c}{1+x^2+y^2}\,, \end{aligned} \tag{25.11}$$

with $a = 0.9$, $b = 0.4$, $c = 6$. The fixed point x_* is located at $(x, y) \approx (0.53275, 0.24689)$, with eigenvalues of the Jacobian matrix $(\Lambda_1, \Lambda_2) \approx (-2.3897, -0.3389)$, so the flow is already stabilized with $\mathbf{C} = \mathbf{1}$. Fig. 25.3 depicts the flow of the vector field around the fixed point x_*.

In order to determine x_*, one needs to integrate the vector field (25.9) forward in time (the convergence is exponential in time), using a fourth order Runge-Kutta or any other integration routine.

In contrast, determination of the 3-cycles of the Ikeda map requires nontrivial $\mathbf{C}$ matrices, different from the identity. Consider for example the hyperbolic fixed point $(x, y) \approx (-0.13529, -0.37559)$ of the third iterate f^3 of the Ikeda map. The flow of the vector field for $\mathbf{C} = \mathbf{1}$, Fig. 25.4(a), indicates a hyperbolic equilibrium point, while for $\mathbf{C} = \left(\begin{smallmatrix} 1 & 0 \\ 0 & -1 \end{smallmatrix}\right)$ the flow of the vector field, fig. 25.4(b) indicates that x_* is an attracting equilibrium point, reached at exponential speed by integration forward in time.

The generalization from searches for fixed points to searches for cycles is straightforward. In order to determine a prime cycle $x = (x_1, x_2, \ldots, x_n)$ of a d-dimensional map $x' = f(x)$, we modify the multipoint shooting method of sect. 14.4.1, and consider the nd-dimensional vector field

$$\frac{dx}{d\tau} = \mathbf{C}\,(f(x) - x)\,, \tag{25.12}$$

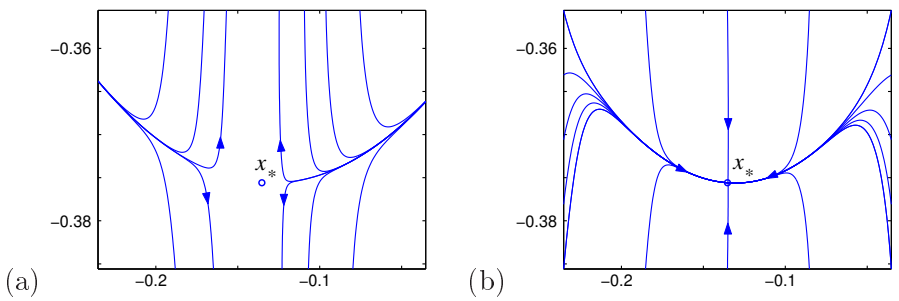

Figure 25.4: Typical trajectories of the vector field (25.10) for a hyperbolic fixed point $(x, y) \approx (-0.13529, -0.37559)$ of f^3, where f is the Ikeda map (25.11). The circle indicates the position of the fixed point. For the vector field corresponding to (*a*) $\mathbf{C} = \mathbf{1}$, x_* is a hyperbolic equilibrium point of the flow, while for (*b*) $\mathbf{C} = \left(\begin{smallmatrix} 1 & 0 \\ 0 & -1 \end{smallmatrix}\right)$, x_* is an attracting equilibrium point.

where $f(x) = (f(x_n), f(x_1), f(x_2), \ldots, f(x_{n-1}))$, and $\mathbf{C}$ is an invertible $[nd \times nd]$ matrix. For the Hénon map, it is sufficient to consider a set of 2^n diagonal matrices with eigenvalues ± 1. Risking a bit of confusion, we denote by x, $f(x)$ both the d-dimensional vectors in (25.10), and nd-dimensional vectors in (25.12), as the structure of the equations is the same.

25.2 Discrete iteration relaxation method

(C. Chandre, F.K. Diakonos and P. Schmelcher)

The problem with the Newton-Raphson iteration (25.2) is that it requires very precise initial guesses. For example, the nth iterate of a unimodal map has as many as 2^n periodic points crammed into the unit interval, so determination of all cycles of length n requires that the initial guess for each one of them has to be accurate to roughly 2^{-n}. This is not much of a problem for 1-dimensional maps, but making a good initial guess for where a cycle might lie in a d-dimensional phase space can be a challenge.

Emboldened by the success of the cyclist relaxation trick (25.8) of manually turning instability into stability by a sign change, we now (*i*) abandon the Newton-Raphson method altogether, (*ii*) abandon the continuous fictitious time flow (25.9) with its time-consuming integration, replacing it by a map g with a larger basin of attraction (not restricted to a linear neighborhood of the fixed point). The idea is to construct a very simple map g, a linear transformation of the original f, for which the fixed point is stable. We replace the Jacobian matrix prefactor in (25.2) (whose inversion can be time-consuming) by a constant matrix prefactor

$$x' = g(x) = x + \Delta\tau \mathbf{C}(f(x) - x), \tag{25.13}$$

where $\Delta\tau$ is a positive real number, and $\mathbf{C}$ is a $[d\times d]$ permutation and reflection matrix with one and only one non-vanishing entry ± 1 per row or column. A fixed point of f is also a fixed point of g. Since $\mathbf{C}$ is invertible, the inverse is also true.

This construction is motivated by the observation that for small $\Delta\tau \to d\tau$ the map (25.13) is the Euler method for integrating the modified flow (25.10), with the integration step $\Delta\tau$.

The argument why a suitable choice of matrix $\mathbf{C}$ can lead to the stabilization of an unstable periodic orbit is similar to the one used to motivate the construction of the modified vector field in sect. 25.1. Indeed, the flow (25.8) is the simplest example of this method, with the infinitesimal fictitious time increment $\Delta\tau \to d\tau$, the infinitesimal coordinate correction $(x - x') \to dx_i$, and the $[n\times n]$ diagonal matrix $\mathbf{C} \to \sigma_i = \pm 1$.

For a given fixed point of $f(x)$ we again chose a $\mathbf{C}$ such that the flow in the expanding directions of $\mathbf{J}(x_*)$ is turned into a contracting flow. The aim is to stabilize x_* by a suitable choice of $\mathbf{C}$. In the case where the map has multiple fixed points, the set of fixed points is obtained by changing the matrix $\mathbf{C}$ (in general different for each unstable fixed point) and varying initial conditions for the map g. For example, for 2-dimensional dissipative maps it can be shown that the 3 matrices

☞ remark 25.3

$$\mathbf{C} \in \left\{ \begin{pmatrix} 1 & 0 \\ 0 & 1 \end{pmatrix}, \begin{pmatrix} -1 & 0 \\ 0 & 1 \end{pmatrix}, \begin{pmatrix} 1 & 0 \\ 0 & -1 \end{pmatrix} \right\}$$

☞ appendix G.2

suffice to stabilize all kinds of possible hyperbolic fixed points.

If $\Delta\tau$ is chosen sufficiently small, the magnitude of the eigenvalues of the fixed point x_* in the transformed system are smaller than one, and one has a stable fixed point. However, $\Delta\tau$ should not be chosen too small: Since the convergence is geometrical with a ratio $1 - \alpha\Delta\tau$ (where the value of constant α depends on the stability of the fixed point in the original system), small $\Delta\tau$ can slow down the speed of convergence. The critical value of $\Delta\tau$, which just suffices to make the fixed point stable, can be read off from the quadratic equations relating the stability coefficients of the original system and those of the transformed system. In practice, one can find the optimal $\Delta\tau$ by iterating the dynamical system stabilized with a given $\mathbf{C}$ and $\Delta\tau$. In general, all starting points converge on the attractor provided $\Delta\tau$ is small enough. If this is not the case, the trajectory either diverges (if $\Delta\tau$ is far too large) or it oscillates in a small section of the phase space (if $\Delta\tau$ is close to its stabilizing value).

The search for the fixed points is now straightforward: A starting point chosen in the global neighborhood of the fixed point iterated with the transformed dynamical system g converges to the fixed point due to its stability.

Numerical investigations show that the domain of attraction of a stabilized fixed point is a rather extended connected area, by no means confined to a linear neighborhood. At times the basin of attraction encompasses the complete phase space of the attractor, so one can be sure to be within the attracting basin of a fixed point regardless of where on the on the attractor on picks the initial condition.

The step size $|g(x) - x|$ decreases exponentially when the trajectory approaches the fixed point. To get the coordinates of the fixed points with a high precision, one therefore needs a large number of iterations for the trajectory which is already in the linear neighborhood of the fixed point. To speed up the convergence of the final part of the approach to a fixed point we recommend a combination of the above approach with the Newton-Raphson method (25.2).

The fixed points of the nth iterate f^n are cycle points of a cycle of period n. If we consider the map

$$x' = g(x) = x + \Delta\tau \mathbf{C}(f^n(x) - x)\,, \tag{25.14}$$

the iterates of g converge to a fixed point provided that $\Delta\tau$ is sufficiently small and $\mathbf{C}$ is a $[d\times d]$ constant matrix chosen such that it stabilizes the flow. As n grows, $\Delta\tau$ has to be chosen smaller and smaller. In the case of the Ikeda map example 25.2 the method works well for $n \leq 20$. As in (25.12), the multipoint shooting method is the method of preference for determining longer cycles. Consider $x = (x_1, x_2, \ldots, x_n)$ and the nd-dimensional map

$$x' = f(x) = (f(x_n), f(x_1), \ldots, f(x_{n-1}))\,.$$

Determining cycles with period n for the d-dimensional f is equivalent to determining fixed points of the multipoint dn-dimensional f. The idea is to construct a matrix $\mathbf{C}$ such that the fixed point of f becomes stable for the map:

$$x' = x + \Delta\tau \mathbf{C}(f(x) - x),$$

where $\mathbf{C}$ is now a $[nd\times nd]$ permutation/reflection matrix with only one non-zero matrix element ± 1 per row or column. For any given matrix $\mathbf{C}$, a certain fraction of the cycles becomes stable and can be found by iterating the transformed map which is now a nd dimensional map.

From a practical point of view, the main advantage of this method compared to the Newton-Raphson method is twofold: (i) the stability matrix

of the flow need not be computed, so there is no large matrix to invert, simplifying considerably the implementation, and (*ii*) empirical basins of attractions for individual **C** are much larger than for the Newton-Raphson method. The price is a reduction in the speed of convergence.

25.3 Least action method

(P. Dahlqvist)

The methods of sects. 25.1 and 25.2 are somewhat *ad hoc*, as for general flows and iterated maps there is no fundamental principle to guide us in chosing the cost function, such as (25.3), to vary.

For Hamiltonian dynamics, we are on much firmer ground; Maupertuis least action principle. You yawn your way through it in every mechanics course - Maupertuis believed that the principle provided a proof of the existence of God - but as we shall now see, it is a very hands-on numerical method for finding cycles.

Indeed, the simplest and numerically most robust method for determining cycles of planar billiards is given by the principle of least action, or equivalently, by extremizing the length of an approximate orbit that visits a given sequence of disks. In contrast to the multipoint shooting method of sect. 14.4.1 which requires variation of $2N$ phase-space points, extremization of a cycle length requires variation of only N bounce positions s_i.

The problem is to find the extremum values of cycle length $L(s)$ where $s = (s_1, \ldots, s_N)$, that is find the roots of $\partial_i L(s) = 0$. Expand to first order

$$\partial_i L(s_0 + \delta s) = \partial_i L(s_0) + \sum_j \partial_i \partial_j L(s_0) \delta s_j + \ldots$$

and use $\mathbf{J}_{ij}(s_0) = \partial_i \partial_j L(s_0)$ in the N-dimensional Newton-Raphson iteration scheme of sect. 14.2.2

25.1 page 479

$$s_i \mapsto s_i - \sum_j \left(\frac{1}{\mathbf{J}(s)} \right)_{ij} \partial_j L(s) \tag{25.15}$$

The extremization is achieved by recursive implementation of the above algorithm, with proviso that if the dynamics is pruned, one also has to check that the final extremal length orbit does not penetrate a billiard wall.

25.2 page 479

As an example, the short periods and stabilities of 3-disk cycles computed this way are listed table 25.3.

14.10 page 277

p	Λ_p	T_p
0	9.898979485566	4.000000000000
1	-1.177145519638$\times 10^{1}$	4.267949192431
01	-1.240948019921$\times 10^{2}$	8.316529485168
001	-1.240542557041$\times 10^{3}$	12.321746616182
011	1.449545074956$\times 10^{3}$	12.580807741032
0001	-1.229570686196$\times 10^{4}$	16.322276474382
0011	1.445997591902$\times 10^{4}$	16.585242906081
0111	-1.707901900894$\times 10^{4}$	16.849071859224
00001	-1.217338387051$\times 10^{5}$	20.322330025739
00011	1.432820951544$\times 10^{5}$	20.585689671758
00101	1.539257907420$\times 10^{5}$	20.638238386018
00111	-1.704107155425$\times 10^{5}$	20.853571517227
01011	-1.799019479426$\times 10^{5}$	20.897369388186
01111	2.010247347433$\times 10^{5}$	21.116994322373
000001	-1.205062923819$\times 10^{6}$	24.322335435738
000011	1.418521622814$\times 10^{6}$	24.585734788507
000101	1.525597448217$\times 10^{6}$	24.638760250323
000111	-1.688624934257$\times 10^{6}$	24.854025100071
001011	-1.796354939785$\times 10^{6}$	24.902167001066
001101	-1.796354939785$\times 10^{6}$	24.902167001066
001111	2.005733106218$\times 10^{6}$	25.121488488111
010111	2.119615015369$\times 10^{6}$	25.165628236279
011111	-2.366378254801$\times 10^{6}$	25.384945785676

Table 25.3: All prime cycles up to 6 bounces for the three-disk fundamental domain, center-to-center separation $R = 6$, disk radius $a = 1$. The columns list the cycle itinerary, its expanding eigenvalue Λ_p, and the length of the orbit (if the velocity=1 this is the same as its period or the action). Note that the two 6 cycles $\overline{001011}$ and $\overline{001101}$ are degenerate due to the time reversal symmetry, but are not related by any discrete spatial symmetry. (Computed by P.E. Rosenqvist.)

Commentary

Remark 25.1 Piece-wise linear maps. The Lozi map (3.12) is linear, and 100,000's of cycles can be easily computed by [2x2] matrix multiplication and inversion.

Remark 25.2 Relaxation method. The relaxation (or gradient) algorithm is one of the methods for solving extremal problems [25.10]. The method described above was introduced by Biham and Wenzel [25.1], who have also generalized it (in the case of the Hénon map) to determination of *all* 2^n cycles of period n, real or complex [25.2]. The applicability and reliability of the method is discussed in detail by Grassberger, Kantz and Moening [25.4], who give examples of the ways in which the method fails: (a) it might reach a limit cycle rather than a equilibrium saddlepoint (that can be remedied by the complex Biham-Wenzel algorithm [25.2]) (b) different symbol sequences can converge to the same cycle (that is, more refined initial conditions might be needed). Furthermore, Hansen (ref. [25.5] and chapter 4. of ref. [1.3]) has pointed out that the method cannot find certain cycles for specific values of the Hénon map parameters.

In practice, the relaxation method for determining periodic orbits of maps appears to be effective almost always, but not always. It is much slower than the multipoint shooting method of sect. 14.4.1, but also much quicker to program, as it does not require evaluation of stability matrices and their inversion. If the complete set of cycles is required, the method has to be supplemented by other methods.

Remark 25.3 Hybrid Newton-Raphson/relaxation methods. The method discussed in sect. 25.2 was introduced by Schmelcher *et al* [25.6]. The method was extended to flows by means of the Poincaré surface of section technique in ref. [25.7]. It is also possible to combine the Newton-Raphson method and (25.13) in the construction of a transformed map [25.11]. In this approach, each step of the iteration scheme is a linear superposition of a step of the stability transformed system and a step of the Newton-Raphson algorithm. Far from the linear neighborhood the weight is dominantly on the globally acting stability transformation algorithm. Close to the fixed point, the steps of the iteration are dominated by the Newton-Raphson procedure.

Remark 25.4 Relation to the Smale horseshoe symbolic dynamics. For a complete horseshoe Hénon repeller (a sufficiently large), such as the one given in fig. 25.2, the signs $\sigma_i \in \{1, -1\}$ are in a 1-to-1 correspondence with the Smale horsheshoe symbolic dynamics $s_i \in \{0, 1\}$:

$$s_i = \begin{cases} 0 & \text{if } \sigma_i = -1\,, \quad x_i < 0 \\ 1 & \text{if } \sigma_i = +1\,, \quad x_i > 0 \end{cases} \quad . \tag{25.16}$$

For arbitrary parameter values with a finite subshift symbolic dynamics or with arbitrarily complicated pruning, the relation of sign sequences $\{\sigma_1, \sigma_2, \cdots, \sigma_n\}$ to the itineraries $\{s_1, s_2, \cdots, s_n\}$ can be much subtler; this is discussed in ref. [25.4].

Remark 25.5 Ikeda map. Ikeda map (25.11) was introduced in ref. [25.9] is a model which exhibits complex dynamics observed in nonlinear optical ring cavities.

Remark 25.6 Relaxation for continuous time flows. For a d-dimensional flow $\dot{x} = v(x)$, the method described above can be extended by considering a Poincaré surface of section. The Poincaré section yields a map f with dimension d-1, and the above discrete iterative maps procedures can be carried out. A method that keeps the trial orbit continuous throughout the calculation is the Newton descent, a variational method for finding periodic orbits of continuous time flows, is described in refs. [25.12, 25.13].

Remark 25.7 Stability ordering. The parameter $\Delta\tau$ in (25.13) is a key quantity here. It is related to the stability of the desired cycle in the transformed system: The more unstable a fixed point is, the smaller $\Delta\tau$ has to be to stabilize it. With increasing cycle periods, the unstable eigenvalue of the stability matrix increases and therefore $\Delta\tau$ has to be reduced to achieve stabilization of all fixed points. In many cases the least unstable cycles of a given period n are of physically most important [25.8]. In this context $\Delta\tau$ operates as a stability filter. It allows the selective stabilization of only those cycles which posses Lyapunov exponents smaller than a cut-off value. If one starts the search for cycles within a given period n with a value $\Delta\tau \approx O(10^{-1})$, and gradually lowers $\Delta\tau$ one obtains the sequence of all unstable orbits of order n sorted with increasing values of their Lyapunov exponents. For the specific choice of $\mathbf{C}$ the relation between $\Delta\tau$ and the stability coefficients of the fixed points of the original system is strictly monotonous. Transformed dynamical systems with other $\mathbf{C}$'s do not obey such a strict behavior but show a rough ordering of the sequence of stability eigenvalues of the fixed points stabilized in the course of decreasing values for $\Delta\tau$. As explained in sect. 15.4, stability ordered cycles are needed to order cycle expansions of dynamical quantities of chaotic systems for which a symbolic dynamics is not known. For such systems, an ordering of cycles with respect to their stability has been proposed [15.13, 15.14, 15.12], and shown to yield good results in practical applications.

☞ sect. 15.4

Remark 25.8 Action extremization method. The action extremization (sect. 25.3) as a numerical method for finding cycles has been

introduced independently by many people. We have learned it from G. Russberg, and from M. Sieber's and F. Steiner's hyperbola billiard computations [25.14, 25.15]. The convergence rate is really impressive, for the Sinai billiard some 5000 cycles are computed within CPU seconds with rather bad initial guesses.

Variational methods are the key ingredient of the Aubry-Mather theory of area-preserving twist maps (known in the condensed matter literature as the Frenkel-Kontorova models of 1-dimensional crystals), discrete-time Hamiltonian dynamical systems particularly suited to explorations of the K.A.M. theorem. Proofs of the Aubry-Mather theorem [25.17] on existence of quasi-periodic solutions are variational. It was quickly realized that the variational methods can also yield reliable, high precision computations of long periodic orbits of twist map models in 2 or more dimensions, needed for K.A.M. renormalization studies [25.16].

A fictitious time gradient flow similar to the one discussed here in sect. 25.1 was introduced by Anegent [25.18] for twist maps, and used by Gole [25.19] in his proof of the Aubry-Mather theorem. Mathematical bounds on the regions of stability of K.A.M. tori are notoriously restrictive compared to the numerical indications, and de la Llave, Falcolini and Tompaidis [25.20, 25.21] have found the gradient flow formulation advantageous both in studies of the analyticity domains of the K.A.M. stability, as well as proving the Aubry-Mather theorem for extended systems (for a pedagogical introduction, see the lattice dynamics section of ref. [25.22]).

All of the twist-maps work is based on extremizing the discrete dynamics version of the action S (in this context sometimes called a "generating function"). However, in their investigations in the complex plane, Falcolini and de la Llave [25.20] do find it useful to minimize instead $S\bar{S}$, analogous to our cost function (25.3).

Résumé

Unlike the Newton-Raphson method, variational methods are very robust. As each step around a cycle is short, they do not suffer from exponential instabilities, and with rather coarse initial guesses one can determine cycles of arbitrary length.

References

[25.1] O. Biham and W. Wenzel, *Phys. Rev. Lett.* **63**, 819 (1989).

[25.2] O. Biham and W. Wenzel, *Phys. Rev.* **A 42**, 4639 (1990).

[25.3] P. Grassberger and H. Kantz, *Phys. Lett. A* **113**, 235 (1985).

[25.4] P. Grassberger, H. Kantz and U. Moening, *J. Phys.* **A 43**, 5217 (1989).

[25.5] K.T. Hansen, *Phys. Lett.* **A 165**, 100 (1992).

[25.6] P. Schmelcher and F.K. Diakonos, *Phys. Rev. Lett.* **78**, 4733 (1997); *Phys. Rev. E* **57**, 2739 (1998).

[25.7] D. Pingel, P. Schmelcher and F.K. Diakonos, O. Biham, *Phys. Rev. E* **64**, 026214 (2001).

[25.8] F. K. Diakonos, P. Schmelcher, O. Biham, *Phys. Rev. Lett.* **81**, 4349 (1998).

[25.9] K. Ikeda, *Opt. Commun.* **30**, 257 (1979).

[25.10] F. Stummel and K. Hainer, *Praktische Mathematik* (Teubner, Stuttgart 1982).

[25.11] R.L. Davidchack and Y.C. Lai, *Phys. Rev. E* **60**, 6172 (1999).

[25.12] P. Cvitanović and Y. Lan, "Turbulent fields and their recurrences", in N. Antoniou, ed., *Proceed. of 10. Intern. Workshop on Multiparticle Production: Correlations and Fluctuations in QCD* (World Scientific, Singapore 2003). `nlin.CD/0308006`

[25.13] Y. Lan and P. Cvitanović, "Variational method for finding periodic orbits in a general flow", submitted to *Phys. Rev.* **E** (August 2003). `nlin.CD/0305008`

[25.14] M. Sieber and F. Steiner, " Quantum Chaos in the Hyperbola Billiard", *Phys. Lett.* **A 148**, 415 (1990).

[25.15] M. Sieber, *The Hyperbola Billiard: A Model for the Semiclassical Quantization of Chaotic Systems*, Ph.D. thesis (Hamburg 1991); DESY report 91-030.

[25.16] H. T. Kook and J. D. Meiss, "Periodic orbits for reversible symplectic mappings", *Physica D* **35**, 65 (1989).

[25.17] J.N. Mather, "Variational construction of orbits of twist difeomorphisms", J. Amer. Math. Soc. **4** 207 (1991).

[25.18] S. B. Angenent, "The periodic orbits of an area preserving twist-map", *Comm. Math. Phys.* **115**, 353 (1988).

[25.19] C. Golé, "A new proof of the Aubry-Mather's theorem", *Math. Z.* **210**, 441 (1992).

[25.20] C. Falcolini and R. de la Llave, "Numerical calculation of domains of analyticity for perturbation theories in the presence of small divisors", *J. Stat. Phys.* **67**, 645 (1992).

[25.21] S. Tompaidis, "Numerical Study of Invariant Sets of a Quasi-periodic Perturbation of a Symplectic Map", *Experimental Mathematics* **5**, 211 (1996).

[25.22] R. de la Llave, *Variational methods for quasiperiodic solutions of partial differential equations*, `mp_arc 00-56`.